

Spiking Neural Network for Intra-cortical Brain Signal Decoding

Song Yang, Haotian Fu, Herui Zhang, Peng Zhang, Wei Li and Dongrui Wu, *Fellow, IEEE*

Abstract—Decoding brain signals accurately and efficiently is crucial for intra-cortical brain-computer interfaces. Traditional decoding approaches based on neural activity vector features suffer from low accuracy, whereas deep learning based approaches have high computational cost. To improve both the decoding accuracy and efficiency, this paper proposes a spiking neural network (SNN) for effective and energy-efficient intra-cortical brain signal decoding. We also propose a feature fusion approach, which integrates the manually extracted neural activity vector features with those extracted by a deep neural network, to further improve the decoding accuracy. Experiments in decoding motor-related intra-cortical brain signals of two rhesus macaques demonstrated that our SNN model achieved higher accuracy than traditional artificial neural networks; more importantly, it was tens or hundreds of times more efficient. The SNN model is very suitable for high precision and low power applications like intra-cortical brain-computer interfaces.

Index Terms—Brain-computer interface, feature fusion, intra-cortical brain signal decoding, spiking neural network

I. INTRODUCTION

Brain-computer interfaces (BCIs) [1], as shown in Fig. 1, establish a direct communication pathway between the brain and external devices. They can be categorized into invasive BCIs, whose electrodes are placed inside the skull, and non-invasive ones, which do not need surgery.

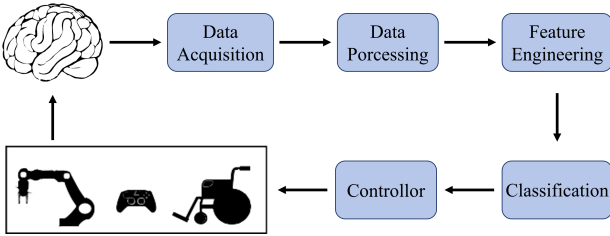


Fig. 1. A closed-loop BCI system.

Non-invasive BCIs can be used for text input [2], neuro-rehabilitation [3], device control [4], etc. Despite their convenience, the input signals of non-invasive BCIs have low spatial resolution and limited information, and hence may not

S. Yang, H. Fu, H. Zhang, W. Li and D. Wu are with the Key Laboratory of the Ministry of Education for Image Processing and Intelligent Control, School of Artificial Intelligence and Automation, Huazhong University of Science and Technology, Wuhan 430074, China. They are also with Hubei Key Laboratory of Brain-inspired Intelligent Systems, Huazhong University of Science and Technology, Wuhan, 430074, China.

P. Zhang is with Department of Biomedical Engineering, College of Life Science and Technology, Huazhong University of Science and Technology, Wuhan 430074, China.

W. Li and D. Wu are the corresponding authors. Email: li-wei0828@hust.edu.cn, drwu09@gmail.com.

be suitable for sophisticated applications like accurate speech decoding [5] and restoring walking abilities of paralyzed patients [6].

Intra-cortical brain-computer interfaces (iBCIs), a type of invasive BCIs that implant electrodes into the cortex, can record much higher quality brain signals, enabling more precise neural signal decoding and more sophisticated BCI applications. iBCIs have demonstrated remarkable capabilities in motor movement interpretation and device control, for both human and non-human primates (NHPs) [7]–[12].

Accurate intra-cortical brain signal decoding is critical for iBCIs. Many existing iBCI decoding approaches use hand-crafted neural activity vector (NAV) features, and linear classifiers/regressors [13], [14]. Deep learning using artificial neural networks (ANNs) has achieved remarkable successes in computer vision [15], speech recognition [16], natural language processing [17], and also non-invasive BCIs [18]–[21]. Spiking neural networks (SNNs), which mimic the authentic communication process of neurons in the human brain, are considered as the third generation of neural networks [22]. Unlike ANNs that perform calculations using continuous numbers, SNNs utilize sparse and discrete spikes. This manner of calculation enables SNNs to achieve lower energy consumption and higher computational efficiency on neuromorphic hardware [23], while maintaining comparable performance with ANNs.

SNNs take spiking signals as input, whereas most iBCIs acquire spiking neural signals. Moreover, low energy consumption is very important for iBCIs to avoid damages to the brain. Therefore, SNNs are very promising for iBCI decoding. Unfortunately, there has not been much research in this direction [12].

This paper proposes a spiking neural network for effective and energy-efficient intra-cortical brain signal decoding. We also propose a feature fusion (FF) approach, which integrates the manually extracted NAV features with those extracted by a deep neural network, to further improve the decoding accuracy. Experiments in decoding motor-related intra-cortical brain signals of two rhesus macaques demonstrated that our SNN model achieved higher accuracy than traditional ANNs; more importantly, it was tens or hundreds of times more efficient.

The remainder of this paper is organized as follows. Section II introduces related works. Section III introduces our proposed SNN and FF approaches. Section IV presents the experiment results. Finally, Section V draws conclusions.

II. RELATED WORKS

This section introduces related works on BCIs, SNNs, and SNN for iBCI decoding.

A. Brain Signal Decoding

ANN-based deep learning has achieved great successes in non-invasive BCIs. Representative approaches include convolutional neural network (CNN) based ShallowConvNet [24], DeepConvNet [24], and EEGNet [25], and Transformer based EEGConFormer [26] and EEGDeformer [27].

Existing iBCI decoding algorithms mostly use traditional machine learning models, instead of deep learning. For example, Chen et al. [13] designed a sparse Bayesian linear regression model to decode 3D movements of non-human primates; Zhang et al. [28] proposed a principal component analysis based algorithm to cope with inter-session discrepancies; Li et al. [29] introduced a thermodynamic model utilizing both local field potentials and spike signals. In human rehabilitation applications, Collinger et al. [14] constructed a neural decoder based on a mathematic model that linearly relates neural firing rates to movement velocities, and calibrated it for several weeks for a 52-year-old patient with tetraplegia. Bradman et al. [30] used a steady-state Kalman filter and Gaussian process regression on three patients with tetraplegia to achieve rapid closed-loop neural cursor control. Flesher et al. [31] found that it is feasible to mimic known biological control principles in a prosthetic arm controlling system.

B. SNNs

Spiking neurons, which mimic the biological neurons in the brain by converting continuous signals into spike trains, are the basic elements of SNNs. The Izhikevich model [32] best approximates the real neurons but suffers from high computational complexity. Simplified neuron models like the quadratic integrate-and-fire (QIF) model [33], the exponential integrate-and-fire (EIF) model [34], the leaky integrate-and-fire (LIF) model [35], and the parametric leaky integrate-and-fire (PLIF) model [36], are more computationally efficient, and hence used more broadly in SNNs.

Unlikely ANNs, which are usually trained by back-propagation [37], training SNNs through back-propagation is infeasible due to the discrete nature of the spikes, which leads to gradient explosion or vanishing. Generally, there are three main training strategies for SNNs: ANN-to-SNN conversion [38], spike-timing-dependent plasticity [39], and surrogate gradient [40].

C. SNNs for iBCIs

Several SNNs have been proposed to decode intra-cortical brain signals.

Dethier et al. [41] designed a simulated SNN model using the neural engineer framework, a general method for mapping control algorithms into SNNs. Boi et al. [42] implemented a spiking network on a compact neuromorphic processor, using the spike-timing-dependent plasticity as the learning method. Their experiments demonstrated the chip's ability to

correctly learn decoding tasks. Zheng et al. [43] utilized an SNN model as data generator, showing that a small amount of training data conforming to neural population dynamics could be generated, thereby enhancing the decoding performance. McMillan et al. [12] introduced an SNN-LSTM structure to decode the movement through brain signals, leveraging both the low energy consumption of SNNs and LSTM's ability to capture long-term temporal dependencies.

This paper proposes an SNN for both low energy consumption and high decoding accuracy.

III. METHODS

This section introduces our proposed SNN and FF approaches.

A. Spiking Neuron and Surrogate Gradient

SNNs transmit information across layers in the form of spike trains through spiking neurons.

For a PLIF neuron [36] with input I_t and membrane potential u_t , its hidden state h_t is updated as:

$$h_t = \beta u_t + (1 - \beta)I_t, \quad t = 1, \dots, T \quad (1)$$

where T is the time step, and $\beta = 1 - \frac{1}{\tau}$, in which τ is a learnable positive time constant to ensure $0 < \beta < 1$.

The neuron output O_t is determined by the Heaviside function H :

$$O_t = H(h_t - V_{th}) = \begin{cases} 1, & \text{if } h_t \geq V_{th} \\ 0, & \text{otherwise} \end{cases}, \quad (2)$$

i.e., it fires a spike when h_t exceeds a threshold V_{th} , and gives no output otherwise.

If the neuron fires, then its membrane potential resets to u_{reset} , which by default is set to 0, i.e.,

$$u_{t+1} = (1 - O_t)h_t + O_t u_{reset}. \quad (3)$$

Fig. 2(a) shows the calculation flow of a PLIF neuron.

Computing the gradients for PLIF neuron based SNNs is challenging, because the Heaviside function is non-differentiable: the gradient becomes infinite at the threshold and zero elsewhere, leading to potential gradient vanishing or explosion. Surrogate gradient [44] has been proposed to address this problem. It replaces the Heaviside function with a surrogate function (typically sigmoid or arctan) in gradient calculation.

Using the sigmoid function $\sigma(\cdot)$ as an example, the gradient calculation becomes:

$$\begin{aligned} \frac{\partial O_t}{\partial h_t} &= \frac{\partial \sigma(h_t - V_{th})}{\partial h_t} \\ &= \sigma(h(t) - V_{th}) \cdot (1 - \sigma(h(t) - V_{th})). \end{aligned} \quad (4)$$

This approach, as Fig. 2(b) shows, ensures the gradient remains finite and nonzero, approximating the original gradient while enabling more stable training.

TABLE I
THE SNN MODEL CONFIGURATION.

Layer	Type	Number of filters	Kernel size	Number of parameters	Output size
Input					(C_{in}, T)
Temporal Convolution (TC)	Conv1D Batch Normalization Parametric LIF	C_{in} C_h $2C_h$	64	$C_{in} \times C_h \times 64$ $2C_h$ $2C_h$	(C_h, T)
Spatial Convolution (SC)	Conv2D Batch Normalization Parametric LIF	1 C_h $2C_h$	(64,1)	64 $2C_h$ $2C_h$	(C_h, T)
Average Pooling					(C_h)
Classifier	Linear			$C \times N_{class}$	(N_{class})

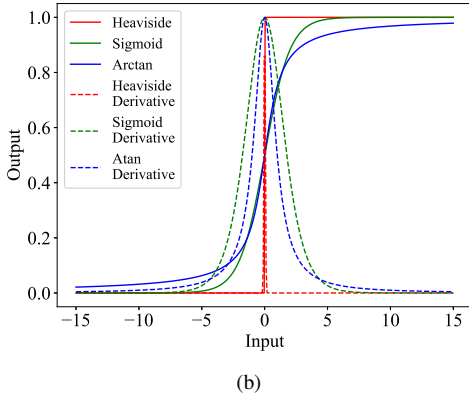
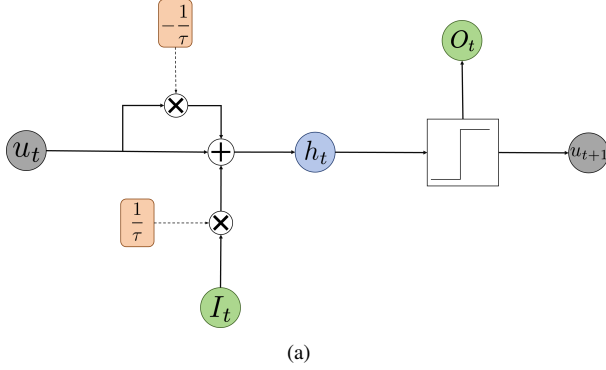


Fig. 2. (a) The computational process of a PLIF neuron. (b) The Heaviside function and two surrogate functions, and their derivatives.

B. Our Proposed SNN

Fig. 3 shows the architecture of our proposed SNN. More specific configurations and the definitions of some variables used in this subsection are given in Table I. Its input has the dimensionality $C \times T$, where C is the number of signal channels and T the number of time domain sampling points. T is also used as the time step in the PLIF neurons.

The SNN includes two main components: a feature extractor and a classifier. The feature extractor comprises a temporal convolution (TC) layer and a spatial convolution (SC) layer. The TC layer performs channel-wise 1D convolution and restructures the input spiking data $X \in \mathbb{R}^{C \times T}$ from C channels to C_h channels, whereas the SC layer performs standard 2D convolution. Each channel calculated by convolution kernels is followed by a 1D batch normalization layer and a PLIF

neuron.

First, the temporal kernel $K_{temp,j} \in \mathbb{R}^{C \times k_{temp}}$, where $j = 1, 2, \dots, C_h$ and k_{temp} is the kernel length of TC, is applied to the input X . This process is:

$$\hat{\mathbf{z}}_j = \text{cov}(K_{temp,j}, X), \quad (5)$$

where cov is the convolution calculation. Denote $\hat{\mathbf{Z}} = [\hat{\mathbf{z}}_1; \hat{\mathbf{z}}_2; \dots; \hat{\mathbf{z}}_{C_h}] \in \mathbb{R}^{C_h \times T}$ as the temporal features calculated by the kernels.

The batch normalization layer performs channel-wise normalization using mean $[\mu_1; \mu_2; \dots; \mu_{C_h}]$ and variance $[\sigma_1; \sigma_2; \dots; \sigma_{C_h}] \in \mathbb{R}^{C_h}$:

$$\bar{\mathbf{z}}_j = \frac{\hat{\mathbf{z}}_j - \mu_j}{\sigma_j}, \quad (6)$$

$$\mathbf{z}_j = \alpha_j \cdot \bar{\mathbf{z}}_j + \xi_j, \quad (7)$$

where α_j and ξ_j are batch normalization parameters to be tuned. This process is denoted as $Z = \text{BN}(\hat{\mathbf{Z}})$.

After the batch normalization layer, the temporal feature of the j -th channel, $\mathbf{z}_j = [z_1, z_2, \dots, z_T]$, is sent to the PLIF neuron to calculate the spike encodings by (1)-(3). For time step $t \in [t_B, t_E]$, where t_B is the time the neuron fires the first spike and t_E is the time the neuron fires the next spike, the hidden state of the neuron is calculated by:

$$\begin{aligned} h_t &= \beta u_t + (1 - \beta) z_t \\ &= \beta^2 u_{t-1} + \beta(1 - \beta) z_{t-1} + (1 - \beta) z_t \\ &\vdots \\ &= \beta^{t-t_B} (1 - \beta) z_{t_B} + \dots + \beta(1 - \beta) z_{t-1} + (1 - \beta) z_t \end{aligned} \quad (8)$$

The firing process is depicted by (2) and (3). The entire calculation flow of the PLIF neuron is denoted as $O = \text{PLIF}(Z)$. Since β is learnable, the PLIF neuron output O can adapt to the input Z .

The temporal-spatial spike features $F \in \mathbb{R}^{C_h \times T}$ are next processed by the SC layer in a manner similar to the TC layer, except that the convolution kernel $K_{spat} \in \mathbb{R}^{1 \times k_{spat}}$ (k_{spat} is the kernel length of SC) is 2D:

$$F = \text{PLIF}(\text{BN}(\text{cov}(K_{spat}, O))). \quad (9)$$

The classifier is a fully connected linear layer with a spiking rate based classification strategy. The spike features F are averaged along the time step dimension to get a feature vector $\mathbf{f} \in \mathbb{R}^{C_h}$ for classification:

$$\hat{\mathbf{y}} = W_c \cdot \mathbf{f}, \quad (10)$$

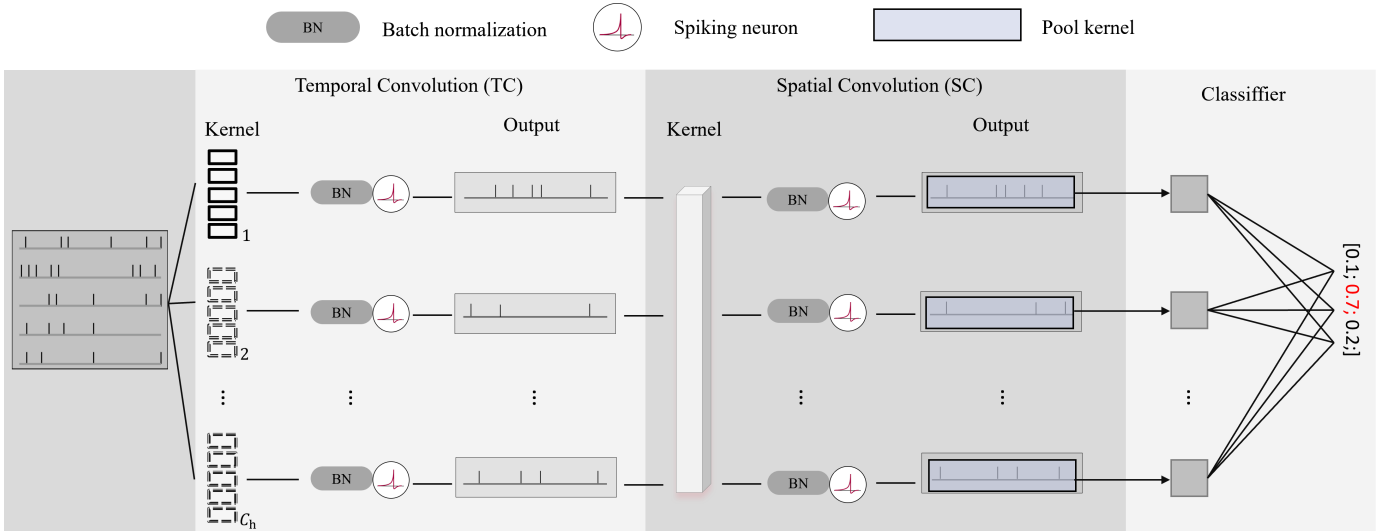


Fig. 3. Architecture of our proposed SNN. The first convolution layer performs channel-wise temporal convolution, with one convolution kernel for each channel. The second layer is spatial convolution to extract the spatial information across different channels. The third layer is a fully connected layer. In each convolution layer, a batch normalization (BN) layer and a PLIF neuron is employed after the kernel.

where $W_c \in \mathbb{R}^{N_{\text{class}} \times C_h}$ is the weight matrix of the classifier, in which N_{class} is the number of classes.

C. Feature Fusion

Prior research [11], [28], [45] has demonstrated the effectiveness of NAV features in decoding movements. Our feature fusion strategy integrates manual NAV features with deep representations extracted by a neural network, as illustrated in Fig. 4.

To compute the NAV features, for each channel we divide the temporal dimension of the spiking input $X \in \mathbb{R}^{C \times T}$ into b non-overlapping segments of length T/b , i.e., $X = [\mathbf{x}_1, \dots, \mathbf{x}_b]$. We then calculate the spike counts for each segment and obtain the b -dimensional NAV features for each channel. The NAV features of different channels are then assembled into feature matrix with dimensionality $C \times b$.

Finally, we project both deep and NAV features into a hidden space and concatenate them. A linear classifier is used to perform the final classification.

IV. EXPERIMENTS

This section performs experiments to demonstrate the effectiveness and efficiency of the proposed SNN and FF approaches. The Python code is available at https://github.com/SongYang008/SNN_iBCIs.

A. Datasets

The intra-cortical neural data were collected in our previous research [28]. The experiment was approved by the Institutional Animal Care and Use Committee at Wuhan University Center for Animal Experiment (No. 2011096) on September 6, 2011.

Two rhesus macaques (Monkey M and Monkey H) performed distinct motor tasks in the experiments, i.e., Monkey M completed a direction reaching task, and Monkey H executed a

shape grasping task (hereafter referred to as reaching task and grasping task), both were three-class classifications. During the experiments, a monkeys sat in front of a panel equipped with objects and target lights, as illustrated in Fig. 5. For the reaching task, three cylindrical objects were positioned at three different locations on the panel: top, top left, and top right. For the grasping task, a single object was positioned at the panel's center, with its shape varied across trials, cycling through cube, triangle, and sphere.

The neural data were acquired using a multi-electrode sensor consisting of three electrode arrays: two 32-channel Utah arrays and one 16-channel FMA array. They were implanted across three critical cortical regions: the primary motor cortex (M1), primary somatosensory cortex (S1), and posterior parietal cortex (PPC). For the grasping task, only 66 arrays were correctly implanted, resulting in a 66-channel dataset. The reaching task had 80 channels.

As shown in Table II, the raw spiking signals were initially sampled at 40 kHz. Each trial consisted of 0.3 second of data, corresponding to 12,000 time points. Each trial was then downsampled to 100 time points by taking the sum of every 120 time points. The reaching task had 14 sessions, each with about 750 trials. The grasping task had 12 sessions, each with 400-1000 trials. Different sessions were collected at different time slots of the same day, or in different days.

TABLE II
CHARACTERISTICS OF THE TWO DATASETS.

Task Type	Sampling Frequency	Number of Sampling Points	Number of Channels	Number of Sessions
Reaching	40 kHz	12,000 \rightarrow 100	80	14
Grasping	40 kHz	12,000 \rightarrow 100	66	12

B. Experiment Settings and Baselines

We used leave-one-session-out cross-validation in our experiments, i.e., one session was used as the test set and all

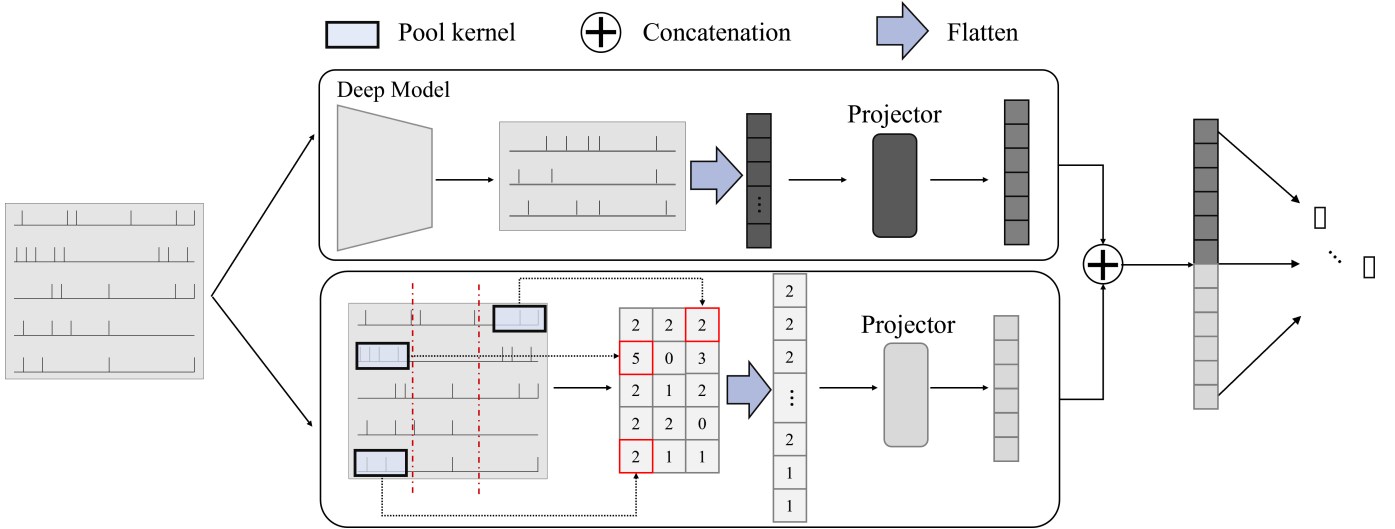


Fig. 4. Feature fusion. We construct a deep neural network (ANN or SNN) and remove its classifier to extract the deep representations. They and the hand-crafted NAV features are then separately and linearly projected into a hidden space. The two projections are concatenated as input to the linear classifier.

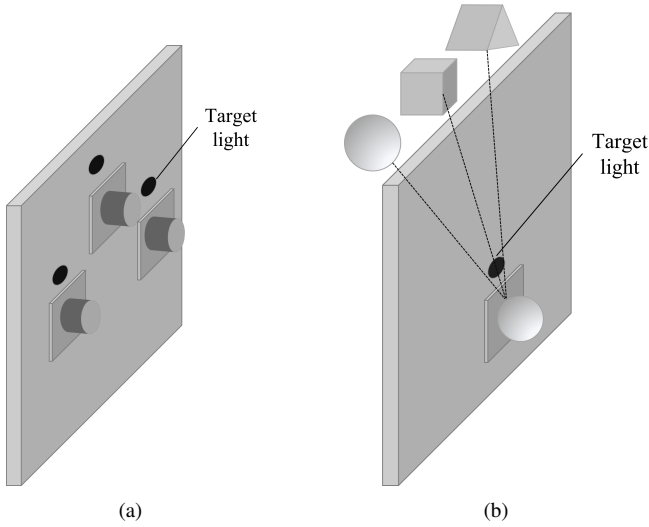


Fig. 5. The neural signal recording settings. (a) The reaching task: Three cylindrical objects were placed on a panel, with a target light positioned above each object. In each trial, the monkey performed a reaching movement guided by the illumination of a specific target light. (b) The grasping task: One of three different shapes (cube, triangle, sphere) was presented at the panel’s center via a motor, for the monkey to grasp.

remaining sessions for training and validation. An 8:2 ratio was used to split the training and validation data. The Adam optimizer with early stopping was used in training, with a maximum of 800 epochs and patience of 100. The initial learning rate was set to 0.001, and the batch size was 256.

The SNN model was implemented using Spikingjelly [46]. The initial β of the PLIF neuron was set to 0.5, and the threshold voltage V_{th} was 1. The hidden channel size C_h of our proposed SNN model was $\frac{C}{2}$, i.e., 40 for the reaching task and 33 for the grasping task. In FF, the dimensionality of the hidden space d was set to 128, and the number of dividing groups $b = 10$.

Five ANN baselines were considered, including EEG-

Net, DeepConvNet, ShallowConvNet, EEGConFormer and EEGDeformer. We repeated the experiments five times with different random seeds and report the average accuracy.

C. Classification Performance

Tables III and IV present the classification results, where the best is marked in bold, and the second best by an underline.

For the reaching task, our model outperformed others in most sessions, and achieved the highest average accuracy (84.25%). EEGConFormer and EEGNet exhibited competitive performance, with average accuracies of 81.79 % and 81.22 %, respectively, but their performance was less consistent than our model.

For the grasping task, our model again excelled in multiple sessions, particularly in difficult ones like sessions 3 and 8. It also achieved the highest average accuracy (91.85 %). EEGNet was the second-best model, with an average accuracy of 90.80 %. EEGConFormer and EEGDeformer also showed competitive performance in certain sessions.

Overall, the reaching task performance showed lower classification accuracy and larger fluctuations than the grasping task, because the former was more complex. However, in both tasks, our proposed SNN achieved the best average performance. Furthermore, t -tests showed that the performance improvements of our proposed SNN model over others were statistically significant ($p < 0.01$).

D. Effectiveness of Feature Fusion

This subsection evaluates the effectiveness of our proposed FF strategy.

First, we investigated the effect of integrating the manually extracted NAV features on both ANN baselines and our proposed SNN model. The results are shown in Table V. FF improved the classification performance in most cases for the ANN baselines. Furthermore, it improved the performance of our SNN model in both scenarios: from 84.25% to 85.19% in

TABLE III
CLASSIFICATION PERFORMANCE OF DIFFERENT MODELS IN THE REACHING TASK.

Session	0	1	2	3	4	5	6	7	8	9	10	11	12	13	Avg
ShallowConvNet	71.70	64.16	92.23	89.28	82.83	84.10	78.80	89.79	67.53	71.50	83.11	77.42	79.18	85.17	79.77 \pm 1.41
DeepConvNet	79.29	63.62	92.50	86.62	85.41	82.07	79.36	87.49	58.92	77.80	78.47	80.28	75.82	80.74	79.17 \pm 1.76
EEGConFormer	65.05	<u>67.92</u>	<u>94.79</u>	90.13	82.86	<u>85.48</u>	81.81	88.76	<u>71.24</u>	81.56	<u>85.21</u>	<u>82.46</u>	73.70	94.09	<u>81.79</u> \pm 2.43
EEGDeformer	<u>78.58</u>	56.74	93.12	90.18	<u>86.06</u>	84.87	75.63	90.21	67.39	<u>82.82</u>	82.60	80.56	71.77	87.74	80.59 \pm 1.68
EEGNet	73.43	66.18	94.36	<u>93.07</u>	89.09	84.46	73.16	<u>90.91</u>	71.80	83.94	86.74	77.52	61.53	<u>90.90</u>	81.22 \pm 2.24
Ours	77.41	69.66	94.84	93.66	90.07	87.19	<u>81.45</u>	92.53	67.59	84.81	89.02	85.55	<u>76.22</u>	90.19	84.25 \pm 1.56

TABLE IV
CLASSIFICATION PERFORMANCE OF DIFFERENT MODELS IN THE GRASPING TASK.

Session	0	1	2	3	4	5	6	7	8	9	10	11	Avg
ShallowConvNet	94.17	<u>94.91</u>	96.33	<u>53.77</u>	<u>91.38</u>	93.98	96.95	96.5	<u>80.97</u>	93.97	82.24	<u>95.14</u>	89.19 \pm tiny1.14
DeepConvNet	93.46	92.53	95.94	50.18	92.28	94.61	97.41	96.76	77.87	93.1	82.58	96.02	88.56 \pm 0.89
EEGConFormer	96.02	97.33	<u>97.00</u>	49.28	92.88	<u>95.81</u>	<u>97.53</u>	96.61	78.25	<u>95.65</u>	85.23	97.64	<u>89.94</u> \pm 1.23
EEGDeformer	<u>95.37</u>	95.83	97.34	53.47	93.62	95.64	98.03	<u>96.76</u>	74.82	95.56	<u>86.00</u>	97.24	89.97 \pm 0.81
EEGNet	94.94	96.35	97.39	57.98	94.39	95.64	97.35	97.12	78.03	95.88	87.34	<u>97.20</u>	90.80 \pm 0.88
Ours	95.68	96.29	97.58	62.00	94.84	96.14	97.97	98.27	80.86	96.06	89.02	97.51	91.85 \pm 0.73

the reaching task, and from 91.78% to 91.82% in the grasping task. These results indicated that the NAV features, which spiking rate related, were generally complementary to the deep learning features.

explaining why it had significant impact on the decoding performance.

TABLE V
CLASSIFICATION ACCURACIES (%) WITH AND WITHOUT FEATURE FUSION.

Backbone	Reaching task		Grasping task	
	w/o FF	w/ FF	w/o FF	w/ FF
ShallowConvNet	79.77	81.20 \uparrow	89.19	90.08 \uparrow
DeepConvNet	79.17	79.36 \uparrow	88.56	90.45 \uparrow
EEGConFormer	81.79	80.71	89.94	90.27 \uparrow
EEGDeformer	80.59	82.03 \uparrow	89.97	90.27 \uparrow
EEGNet	81.22	80.73	90.80	91.15 \uparrow
Ours	84.25	85.19 \uparrow	91.78	91.82 \uparrow

Next, we investigated the effect of the linear feature projectors, i.e., P_{DF} for the deep features and P_{NAV} for the NAV features. Table VI shows the results. Both projectors improved the classification accuracies in both tasks.

TABLE VI
CLASSIFICATION ACCURACIES (%) WITH AND WITHOUT THE LINEAR PROJECTORS.

Model	Reaching task	Grasping task
w/o P_{DF} & P_{NAV}	84.55	91.28
w/ P_{DF}	84.89	91.68
w/ P_{NAV}	84.33	91.53
w/ P_{DF} & P_{NAV}	85.19	91.82

E. Ablation Studies

Ablation studies were performed to investigate the contribution of each module in our proposed SNN model.

First, we examined the role of each convolution layer. Fig. 6(a) shows the results. Removing either TC or SC layer degraded the classification accuracy, particularly the TC layer. Fig. 7 further uses t -distributed stochastic neighbor embedding (t -SNE) [47] to visualize the feature distributions after removing the TC or SC layer. It is clear that features from different classes mixed together when the TC layer was removed,

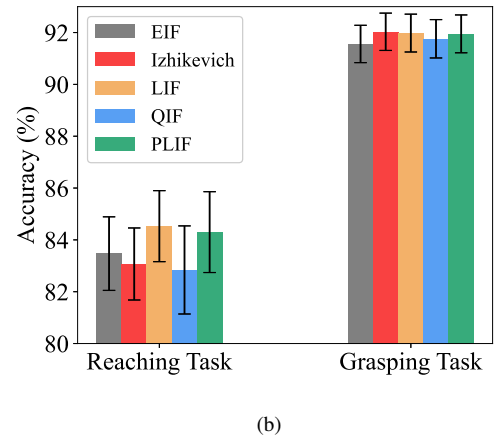
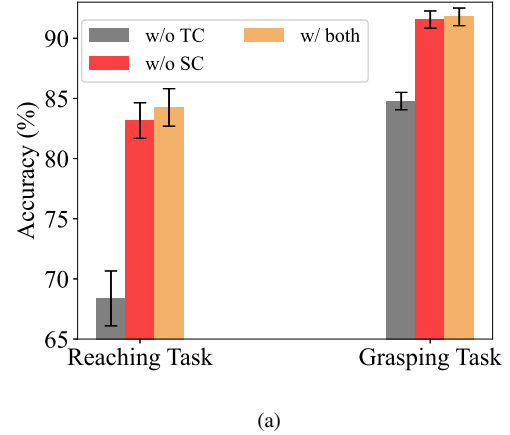


Fig. 6. Classification accuracies in ablation studies. (a) The TC and SC layers; and, (b) different spiking neurons.

Next, we replaced the PLIF neuron with alternative spiking neurons, including LIF, QIF, EIF and Izhikevich neurons. As



Fig. 7. t -SNE visualization of the first session in the reaching and grasping tasks when removing TC or SC.

shown in Fig. 6(b), PLIF and LIF neurons had the best performance, and they were also the most computationally efficient spiking neurons among the five. Between the two, SNN using the PLIF neuron converged faster in our experiments, so we used it in our model.

F. Energy Consumption Analysis

As in prior works [48], [49], we estimated energy consumption under specific constraints: utilizing 32-bit float-point format data and simulating deployment on a 45-nm technology chip [50]. The energy consumption was $E_{\text{MAC}} = 4.6 \text{ pJ}$ for multiplication and accumulation (MAC) operations and $E_{\text{AC}} = 0.9 \text{ pJ}$ for accumulation (AC) operations.

The difference between ANNs and SNNs is that ANNs perform MAC operations, whereas SNNs perform AC operations when taking spiking inputs. For a convolution layer with kernel length k , C_{out} output channels, and input with dimensionality $C_{\text{in}} \times T$, where C_{in} is the number of input channels, the number of AC operations of an SNN is:

$$N_{\text{AC}}^{\text{Cov}} = C_{\text{in}} \cdot C_{\text{out}} \cdot T \cdot k \cdot r, \quad (11)$$

where r is the firing rate of the input spike train.

The number of MAC operations of an ANN is:

$$N_{\text{MAC}}^{\text{Cov}} = C_{\text{in}} \cdot C_{\text{out}} \cdot T \cdot k. \quad (12)$$

Assume the input to the batch normalization layer and PLIF neuron has dimensionality $C \times T$. The number of MAC operations is:

$$N_{\text{MAC}}^{\text{BN}} = N_{\text{MAC}}^{\text{PLIF}} = 2 \cdot C \cdot T. \quad (13)$$

In FF, two linear projectors are adopted. The number of MAC operations is:

$$N_{\text{MAC}}^{\text{FF}} = C \cdot T \cdot d \cdot \frac{1}{b} + C_{\text{h}} \cdot d. \quad (14)$$

The classifier is a fully connected layer. The input dimensionality equals the feature length d_{f} , and the output dimensionality is the number of classes N_{class} . The number of MAC operations is:

$$N_{\text{MAC}}^{\text{C}} = d_{\text{f}} \cdot N_{\text{class}}. \quad (15)$$

The total energy consumption is hence:

$$E = E_{\text{MAC}} \cdot N_{\text{MAC}} + E_{\text{AC}} \cdot N_{\text{AC}}. \quad (16)$$

The energy consumption of an ANN is fixed once the network architecture and input dimensionalities are determined, as the number of MAC and AC operations are determined. In contrast, the energy consumption of an SNN is related to the firing rate, which changes with different inputs. To calculate it more precisely, we calculate the energy consumption of the ANN baselines using an initial model with fixed parameters. For our proposed SNN model, we calculate the average energy consumption based on all samples in the test set.

The results in Table VII demonstrate the superior energy efficiency of our SNN model. It was at least 35 times more efficient than the ANNs in the reaching task, and at least 59 times more efficient than the ANNs in the grasping task.

G. Parameter Sensitivity

In previous experiments, we set the number of hidden channels $C_{\text{h}} = \frac{C_{\text{in}}}{2}$, and the hidden dimensionality $d = 128$ in FF. This subsection investigates their impact to the classification performance.

We varied C_{h} from $C_{\text{in}}/4$ to $2C_{\text{in}}$, i.e., from 20 to 160 in the reaching task and from 16 to 132 in the grasping task. The results are shown in Fig. 8. Increasing C_{h} improved performance, but also led to higher energy consumption. We recommend selecting $C_{\text{h}} \in [C_{\text{in}}/2, C_{\text{in}}]$ to balance the classification performance and efficiency.

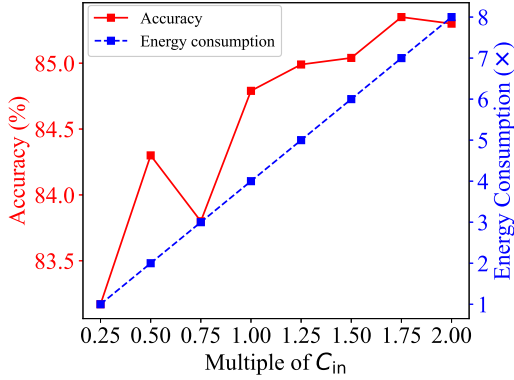
We varied d from 32 to 256. Fig. 9 shows the results. The decoding performance was relatively stable for a wide range of d .

V. CONCLUSIONS

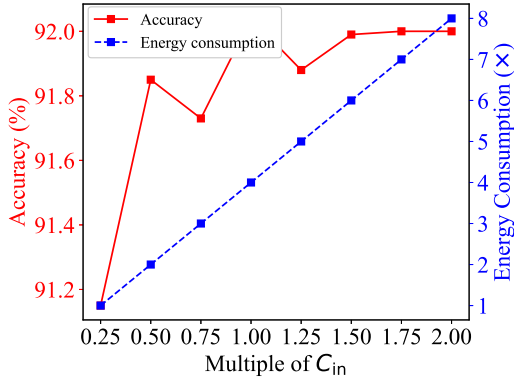
This paper has proposed a spiking neural network architecture for intra-cortical brain signal classification. It consists of a temporal convolution layer and a spatial convolution layer. A batch normalization layer and PLIF spiking neurons are added to each convolution layer. Finally, spike firing rate based features are extracted for classification. We also propose an FF approach, which integrates the manually extracted NAV features with those extracted by a deep neural network,

TABLE VII
ENERGY ESTIMATION

Model	Reaching Task				Grasping Task			
	Params	MAC (M)	AC (K)	Energy Consumption (μJ)	Params	MAC (M)	AC (M)	Energy Consumption (μJ)
ShallowConvNet	129,243	16.16	0	73.88 (131 \times)	106,843	13.33	0	60.95 (217 \times)
DeepConvNet	228,178	109.75	0	504.39 (898 \times)	211,378	90.30	0	415.01 (1480 \times)
EEGConvFormer	217,891	23.87	0	109.34 (194 \times)	222,819	29.32	0	134.55 (480 \times)
EEGDeformer	559,803	7.55	0	33.90 (60 \times)	502,459	7.37	0	33.90 (120 \times)
EEGNet	2,531	4.47	0	20.10 (35 \times)	2,307	3.67	0	16.61 (59 \times)
Ours	205,193	0.32	0.49	0.56 (1\times) *	139,729	0.27	0.17	0.28 (1\times)



(a)



(b)

Fig. 8. Classification accuracies and normalized energy consumption in the (a) reaching task and (b) grasping task when C_h varied.

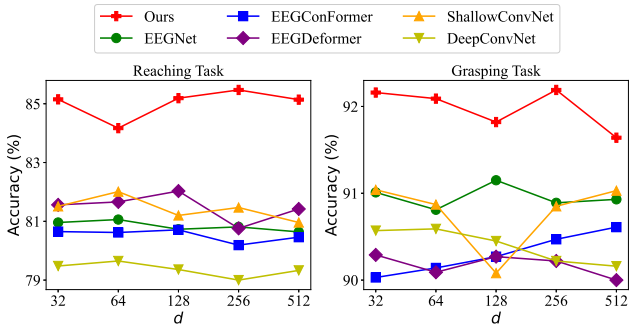


Fig. 9. Classification accuracies when the hidden projection dimensionality d in FF varied.

to further improve the decoding accuracy. Experiments on decoding motor-related intra-cortical brain signals of two rhesus macaques demonstrated that our SNN model had higher accuracy than traditional ANNs; more importantly, it was tens or hundreds of times more efficient.

REFERENCES

- [1] J. R. Wolpaw, N. Birbaumer, D. J. McFarland, G. Pfurtscheller, and T. M. Vaughan, "Brain-computer interfaces for communication and control," *Clinical neurophysiology*, vol. 113, no. 6, pp. 767–791, 2002.
- [2] M. Nakanishi, Y. Wang, C. Wei, K. Chiang, and T. Jung, "Facilitating calibration in high-speed BCI spellers via leveraging cross-device shared latent responses," *IEEE Trans. on Biomedical Engineering*, vol. 67, no. 4, pp. 1105–1113, 2020.
- [3] R. Mane, T. Chouhan, and C. Guan, "BCI for stroke rehabilitation: motor and beyond," *Journal of neural engineering*, vol. 17, no. 4, p. 041001, 2020.
- [4] R. Leeb, D. Friedman, G. R. Müller-Putz, R. Scherer, M. Slater, and G. Pfurtscheller, "Self-paced (asynchronous) BCI control of a wheelchair in virtual environments: a case study with a tetraplegic," *Computational Intelligence and Neuroscience*, vol. 2007, no. 1, p. 079642, 2007.
- [5] D. A. Moses, S. L. Metzger, J. R. Liu, G. K. Anumanchipalli, J. G. Makin, P. F. Sun, J. Chartier, M. E. Dougherty, P. M. Liu, G. M. Abrams *et al.*, "Neuroprosthesis for decoding speech in a paralyzed person with anarthria," *New England Journal of Medicine*, vol. 385, no. 3, pp. 217–227, 2021.
- [6] H. Lorach, A. Galvez, V. Spagnolo, F. Martel, S. Karakas, N. Interling, M. Vat, O. Faivre, C. Harte, S. Komi *et al.*, "Walking naturally after spinal cord injury using a brain-spine interface," *Nature*, vol. 618, no. 7963, pp. 126–133, 2023.
- [7] J. Dethier, P. Nuyujukian, C. Eliasmith, T. Stewart, S. Elasaad, K. V. Shenoy, and K. A. Boahen, "A Brain-Machine Interface operating with a real-time Spiking Neural Network control algorithm," in *Proc. Advance in Neural Information Processing Systems*, Granada, Spain, Dec. 2011, pp. 2213–2221.
- [8] S. Dangi, S. Gowda, R. Heliot, and J. M. Carmena, "Adaptive kalman filtering for closed-loop brain-machine interface systems," in *Int'l. IEEE/EMBS Conf. Neural Engineering*, Cancun, Mexico, Apr. 2011, pp. 609–612.
- [9] L. R. Hochberg, D. Bacher, B. Jarosiewicz, N. Y. Masse, J. D. Simeral, J. Vogel, S. Haddadin, J. Liu, S. S. Cash, P. Van Der Smagt *et al.*, "Reach and grasp by people with tetraplegia using a neurally controlled robotic arm," *Nature*, vol. 485, no. 7398, pp. 372–375, 2012.
- [10] B. P. Christie, D. M. Tat, Z. T. Irwin, V. Gilja, P. Nuyujukian, J. D. Foster, S. I. Ryu, K. V. Shenoy, D. E. Thompson, and C. A. Chestek, "Comparison of spike sorting and thresholding of voltage waveforms for intracortical Brain-Machine Interface performance," *Journal of Neural Engineering*, vol. 12, p. 016009, 2014.
- [11] Y. Dong, S. Wang, Q. Huang, R. W. Berg, G. Li, and J. He, "Neural decoding for intracortical brain-computer interfaces," *Cyborg and Bionic Systems*, vol. 4, p. 0044, 2023.
- [12] K. McMillan, R. Q. So, C. Libedinsky, K. K. Ang, and B. Premchand, "Spike-weighted Spiking Neural Network with spiking long short-term memory: A biomimetic approach to decoding brain signals," *Algorithms*, vol. 17, no. 4, p. 156, 2024.
- [13] Z. Chen and K. Takahashi, "Sparse bayesian inference methods for decoding 3D reach and grasp kinematics and joint angles with primary motor cortical ensembles," in *Proc. Annual Int'l Conf. IEEE Engineering Medicine Biology Society*, Osaka, Japan, Jul. 2013, pp. 5930–5933.

- [14] J. L. Collinger, B. Wodlinger, J. E. Downey, W. Wang, E. C. Tyler-Kabara, D. J. Weber, A. J. McMorland, M. Velliste, M. L. Boninger, and A. B. Schwartz, "High-performance neuroprosthetic control by an individual with tetraplegia," *The Lancet*, vol. 381, no. 9866, pp. 557–564, 2013.
- [15] A. Krizhevsky, I. Sutskever, and G. E. Hinton, "Imagenet classification with deep convolutional neural networks," in *Proc. Advance in Neural Information Processing Systems*, Lake Tahoe, Nevada, USA, Dec. 2012.
- [16] A. Graves, A.-r. Mohamed, and G. Hinton, "Speech recognition with deep recurrent neural networks," in *Proc. IEEE Int'l Conf. Acoustics, Speech and Signal Processing*, Vancouver, Canada, May 2013, pp. 6645–6649.
- [17] J. Devlin, M.-W. Chang, K. Lee, and K. Toutanova, "BERT: Pre-training of deep bidirectional transformers for language understanding," in *Proc. Conf. the North American Chapter of the Association for Computational Linguistics*, Minneapolis, Minnesota, Jun. 2019, pp. 4171–4186.
- [18] D. Wu, B.-L. Lu, B. Hu, and Z. Zeng, "Affective brain-computer interfaces (aBCIs): A tutorial," *Proc. of the IEEE*, vol. 11, no. 10, pp. 1314–1332, 2023.
- [19] X. Chen, Z. Wang, and D. Wu, "Alignment-based adversarial training (ABAT) for improving the robustness and accuracy of EEG-based BCIs," *IEEE Trans. on Neural Systems and Rehabilitation Engineering*, vol. 32, pp. 1703–1714, 2024.
- [20] S. Li, Z. Wang, H. Luo, L. Ding, and D. Wu, "T-TIME: Test-time information maximization ensemble for plug-and-play BCIs," *IEEE Trans. on Biomedical Engineering*, vol. 17, no. 2, pp. 423–432, 2024.
- [21] Z. Wang, S. Li, and D. Wu, "Canine eeg helps human: Cross-species and cross-modality epileptic seizure detection via multi-space alignment," *National Science Review*, 2025, in press.
- [22] W. Maass, "Networks of spiking neurons: the third generation of neural network models," *Neural Netw.*, vol. 10, no. 9, pp. 1659–1671, 1997.
- [23] M. Davies, N. Srinivasa, T.-H. Lin, G. Chinya, Y. Cao, S. H. Choday, G. Dimou, P. Joshi, N. Imam, S. Jain *et al.*, "Loihi: A neuromorphic manycore processor with on-chip learning," *IEEE Micro*, vol. 38, no. 1, pp. 82–99, 2018.
- [24] R. Schirmer, L. Gemein, K. Eggenberger, F. Hutter, and T. Ball, "Deep learning with convolutional neural networks for decoding and visualization of EEG pathology," in *Proc. IEEE Signal Processing in Medicine and Biology Symposium*, Philadelphia, Pennsylvania, USA, Dec. 2017, pp. 1–7.
- [25] V. J. Lawhern, A. J. Solon, N. R. Waytowich, S. M. Gordon, C. P. Hung, and B. J. Lance, "EEGNet: A compact convolutional neural network for EEG-based Brain-Computer Interfaces," *Journal of Neural Engineering*, vol. 15, no. 5, 2018.
- [26] Y. Song, Q. Zheng, B. Liu, and X. Gao, "EEG conformer: Convolutional transformer for EEG decoding and visualization," *IEEE Trans. Neural Systems Rehabilitation Engineering*, vol. 31, pp. 710–719, 2022.
- [27] Y. Ding, Y. Li, H. Sun, R. Liu, C. Tong, C. Liu, X. Zhou, and C. Guan, "EEG-deformer: A dense convolutional transformer for brain-computer interfaces," *IEEE Journal Biomedical and Health Informatics*, pp. 1–10, 2024.
- [28] P. Zhang, X. Ma, L. Chen, J. Zhou, C. Wang, W. Li, and J. He, "Decoder calibration with ultra small current sample set for intracortical brain-machine interface," *Journal of Neural Engineering*, vol. 15, no. 2, p. 056013, 2018.
- [29] W. Li, C. Zhou, X. Chen, H. Mao, J. He, Q. Li, and P. Zhang, "A thermophysical mechanism exploration of the brain: motor cortex modeling with canonical ensemble theory," *Neurocomputing*, p. 128597, 2024.
- [30] D. M. Brandman, T. Hosman, J. Saab, M. C. Burkhart, B. E. Shanahan, J. G. Ciancibello, A. A. Sarma, D. J. Milstein, C. E. Vargas-Irwin, B. Franco *et al.*, "Rapid calibration of an intracortical brain-computer interface for people with tetraplegia," *Journal of Neural Engineering*, vol. 15, no. 2, p. 026007, 2018.
- [31] S. N. Flesher, J. E. Downey, J. M. Weiss, C. L. Hughes, A. J. Herrera, E. C. Tyler-Kabara, M. L. Boninger, J. L. Collinger, and R. A. Gaunt, "A brain-computer interface that evokes tactile sensations improves robotic arm control," *Science*, vol. 372, no. 6544, pp. 831–836, 2021.
- [32] E. M. Izhikevich, "Which model to use for cortical spiking neurons?" *IEEE Trans. Neural Networks*, vol. 15, no. 5, pp. 1063–1070, 2004.
- [33] P. E. Latham, B. Richmond, P. Nelson, and S. Nirenberg, "Intrinsic dynamics in neuronal networks. i. theory," *Journal of Neurophysiology*, vol. 83, no. 2, pp. 808–827, 2000.
- [34] N. Fourcaud-Trocmé, D. Hansel, C. Van Vreeswijk, and N. Brunel, "How spike generation mechanisms determine the neuronal response to fluctuating inputs," *Journal of Neuroscience*, vol. 23, no. 37, pp. 11 628–11 640, 2003.
- [35] L. É. Lapique, "Louis lapique," *Journal of Physiology*, vol. 9, pp. 620–635, 1907.
- [36] W. Fang, Z. Yu, Y. Chen, T. Masquelier, T. Huang, and Y. Tian, "Incorporating learnable membrane time constant to enhance learning of Spiking Neural Networks," in *Proc. IEEE/CVF Int'l. Conf. Computer Vision*, Montreal, Canada, Oct. 2021, pp. 2661–2671.
- [37] D. E. Rumelhart, G. E. Hinton, and R. J. Williams, "Learning representations by back-propagating errors," *Nature*, vol. 323, pp. 533–536, 1986.
- [38] P. U. Diehl, D. Neil, J. Binas, M. Cook, S.-C. Liu, and M. Pfeiffer, "Fast-classifying, high-accuracy spiking deep networks through weight and threshold balancing," in *Proc. Int'l Joint Conf. Neural Networks*, Killarney, Ireland, Jul. 2015, pp. 1–8.
- [39] N. Caporale and Y. Dan, "Spike Timing-Dependent Plasticity: a hebbian learning rule," *Annual review of neuroscience*, vol. 31, no. 1, pp. 25–46, 2008.
- [40] Y. Wu, L. Deng, G. Li, J. Zhu, and L. Shi, "Spatio-temporal backpropagation for training high-performance Spiking Neural Networks," *Frontiers in Neuroscience*, vol. 12, p. 331, 2018.
- [41] J. Dethier, P. Nuyujukian, S. I. Ryu, K. V. Shenoy, and K. Boahen, "Design and validation of a real-time Spiking-Neural-Network decoder for brain-machine interfaces," *Journal of Neural Engineering*, vol. 10, no. 3, p. 036008, 2013.
- [42] F. Boi, T. Moraitis, V. De Feo, F. Diotalevi, C. Bartolozzi, G. Indiveri, and A. Vato, "A bidirectional brain-machine interface featuring a neuro-morphic hardware decoder," *Frontiers in Neuroscience*, vol. 10, p. 563, 2016.
- [43] S. Zheng, W. Li, L. Qian, C. He, and X. Li, "A spiking neural network based on neural manifold for augmenting intracortical brain-computer interface data," in *Proc. Int'l Conf. Artificial Neural Networks*, Bristol, UK, Sep. 2022, pp. 519–530.
- [44] E. O. Neftci, H. Mostafa, and F. Zenke, "Surrogate gradient learning in spiking neural networks: Bringing the power of gradient-based optimization to spiking neural networks," *IEEE Signal Processing Magazine*, vol. 36, no. 6, pp. 51–63, 2019.
- [45] J. Hu, J. Si, B. P. Olson, and J. He, "Feature detection in motor cortical spikes by principal component analysis," *IEEE Trans. Neural Systems Rehabilitation Engineering*, vol. 13, no. 3, pp. 256–262, 2005.
- [46] W. Fang, Y. Chen, J. Ding, Z. Yu, T. Masquelier, D. Chen, L. Huang, H. Zhou, G. Li, and Y. Tian, "Spikingjelly: An open-source machine learning infrastructure platform for spike-based intelligence," *Science Advance*, vol. 9, no. 40, p. eadi1480, 2023.
- [47] L. van der Maaten and G. Hinton, "Visualizing data using t-SNE," *Journal of Machine Learning Research*, vol. 9, pp. 2579–2605, 2008.
- [48] B. Yin, F. Corradi, and S. M. Bohté, "Accurate and efficient time-domain classification with adaptive spiking recurrent neural networks," *Nature Machine Intelligence*, vol. 3, no. 10, pp. 905–913, 2021.
- [49] M. Yao, G. Zhao, H. Zhang, Y. Hu, L. Deng, Y. Tian, B. Xu, and G. Li, "Attention spiking neural networks," *IEEE Trans. Pattern Analysis and Machine Intelligence*, vol. 45, no. 8, pp. 9393–9410, 2023.
- [50] M. Horowitz, "1.1 computing's energy problem (and what we can do about it)," in *Proc. IEEE Int'l Solid-state Circuits Conf.*, San Francisco, California, USA, Feb. 2014, pp. 10–14.

